nature climate change

LETTERS

PUBLISHED ONLINE: 5 JANUARY 2015 | DOI: 10.1038/NCLIMATE2472

Flood risk of natural and embanked landscapes on the Ganges–Brahmaputra tidal delta plain

L. W. Auerbach[1], S. L. Goodbred Jr[1]*, D. R. Mondal[2], C. A. Wilson[1], K. R. Ahmed[3], K. Roy[3], M. S. Steckler[4], C. Small[4], J. M. Gilligan[1] and B. A. Ackerly[5]

The Ganges–Brahmaputra river delta, with 170 million people and a vast, low-lying coastal plain, is perceived to be at great risk of increased flooding and submergence from sea-level rise[1–5]. However, human alteration of the landscape can create similar risks to sea-level rise. Here, we report that islands in southwest Bangladesh, enclosed by embankments in the 1960s, have lost 1.0–1.5 m of elevation, whereas the neighbouring Sundarban mangrove forest has remained comparatively stable[6–8]. We attribute this elevation loss to interruption of sedimentation inside the embankments, combined with accelerated compaction, removal of forest biomass, and a regionally increased tidal range. One major consequence of this elevation loss occurred in 2009 when the embankments of several large islands failed during Cyclone Aila, leaving large areas of land tidally inundated for up to two years until embankments were repaired. Despite sustained human suffering during this time[9,10], the newly reconnected landscape received tens of centimetres of tidally deposited sediment, equivalent to decades' worth of normal sedimentation. Although many areas still lie well below mean high water and remain at risk of severe flooding, we conclude that elevation recovery may be possible through controlled embankment breaches.

Although the risks of climate change and sea-level rise to fluvial delta systems are widely recognized[1,2,11,12], our scientific understanding of the local conditions and processes within these complex landscapes is incomplete[1,11,13]. If we consider the Ganges–Brahmaputra delta as a single unit, then effective dispersal of the river's one gigaton of sediment across the 150,000 km^2 of terrestrial and marine delta can account for ~0.5 cm yr^{-1} of sediment aggradation, which is roughly equivalent to the rate of relative sea-level (RSL) rise measured at several of the area's tide gauges[3,14]. In reality, though, rates of sedimentation are not evenly distributed across the delta[15], nor are rates of RSL change owing to differences in subsidence, compaction and alterations of the tidal regime[14,16]. Understanding these local patterns and controls is essential to effective and realistic management of these regions.

The west-central Ganges–Brahmaputra delta plain of Bangladesh has been effectively cut off from fluvial sediment owing to eastward migration of the Ganges river over the past several thousand years[17]. Yet this 'abandoned' portion of the delta has remained largely stable owing to sediment input from ephemeral distributaries and silt-laden plumes advected onshore by tides extending >100 km inland[8,14,18,19]. The jewel of this vast intertidal landscape is the Sundarban mangrove forest, a 10,000 km^2 UNESCO World Heritage site and home to the largest population of Royal Bengal tigers (Supplementary Fig. 1). With an annual land loss of ~0.04% over the past two centuries (~4 km^2 yr^{-1} balanced by a net gain of 12 km^2 yr^{-1} in the eastern delta)[20], the physical environment of the Sundarbans and the Ganges–Brahmaputra delta remains relatively robust, with no major land loss or conversion to open water such as that occurring in the Mississippi and Nile delta systems[20–22].

Bordering the Sundarbans to the north, though, is the starkly contrasting, human-modified environment of southwest Bangladesh, which comprises more than 50 large islands, formerly forested and intertidal. The islands were cleared over time and ultimately embanked in the 1960s and 1970s as part of a successful effort to boost food production by increasing arable land for rice cultivation[23]. Referred to by the Dutch term polder, these islands are artificially protected from tidal and storm-surge inundation by earthen embankments constructed around their margins. However, in addition to stemming floodwater, the embankments also preclude the deposition of sediment that normally sustains the elevation of the landscape. Such elevation loss, plus deteriorating drainage and other problems, followed embankment construction in many locations, but the controlled breaching of embankments has been reported to restore elevation and relieve environmental problems in some sites[23]. However, there has not been a detailed scientific study of this process.

In May 2012, a fast-static GPS (Global Positioning System) and theodolite survey of land-surface elevations was conducted on Polder 32, a 60-km^2 island in southwest Bangladesh, including measurements from the adjacent Sundarban forest (Fig. 1). Results show that mean elevation of the Sundarbans near Polder 32 is 2.65 ± 0.10 m relative to the EGM96 datum, which lies just above the mean high water (MHW) of 2.55 ± 0.10 m measured at this location (Fig. 2 and Supplementary Figs 2–5). These elevations and the relationship with MHW are consistent with observations elsewhere in the Sundarbans, which show an equilibrium elevation of 2.35–2.85 m EGM96 near the upper third of high-tide levels[24]. In contrast, mean elevation of the Polder 32 land surface is just 1.50 ± 0.10 m, which is ~115 cm lower than that of the Sundarbans and, more significantly, lies ~105 cm below MHW levels in the surrounding tidal channels (Fig. 2). This elevation disparity between the natural and poldered landscapes represents ~2 cm yr^{-1} of relative elevation change over the five decades since polder construction, equating to an effective rate of sea-level rise that is more than double the upper end of Intergovernmental Panel on Climate Change projections[2].

[1]Department of Earth and Environmental Sciences, Vanderbilt University, Nashville, Tennessee 37240, USA. [2]School of Earth and Environmental Sciences, Queens College—City University of New York, Queens, New York 11367, USA. [3]Environmental Science Discipline, Khulna University, Khulna 9208, Bangladesh. [4]Lamont-Doherty Earth Observatory, Columbia University, Palisades, New York 10964, USA. [5]Department of Political Science, Vanderbilt University, Nashville, Tennessee 37203, USA. *e-mail: steven.goodbred@vanderbilt.edu

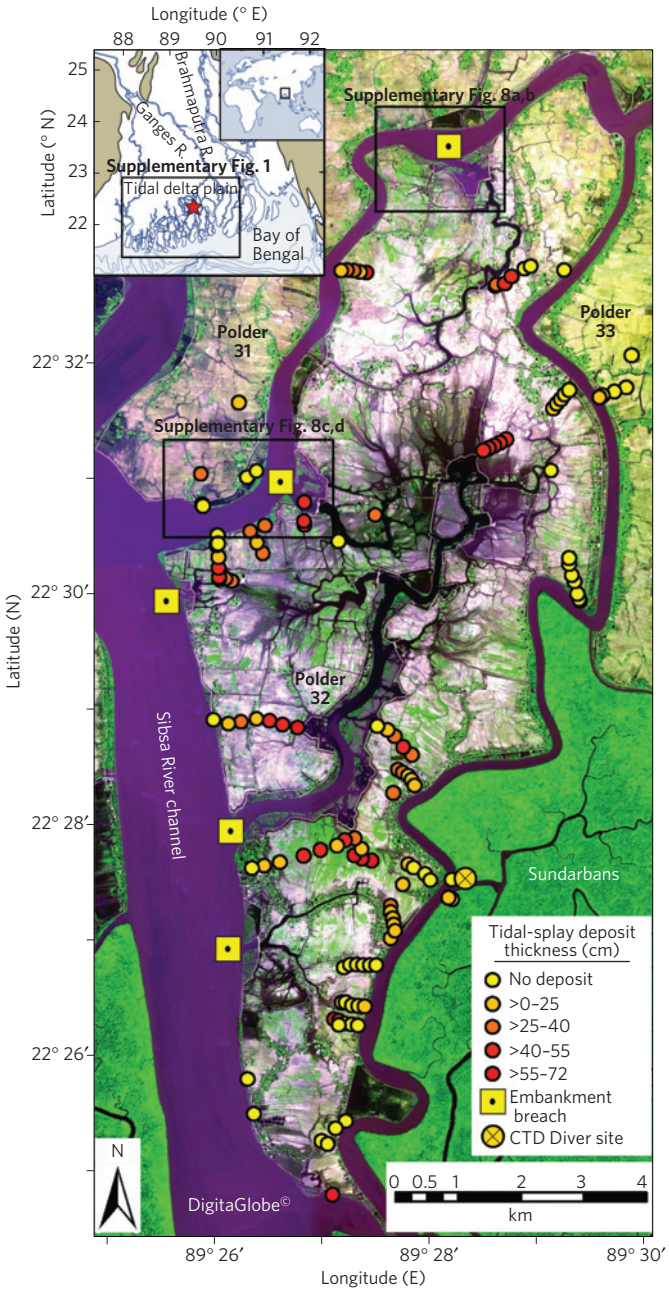

Figure 1 | DigitalGlobe image of Polder 32 located on the tidal delta plain of southwest Bangladesh, collected in May 2012, three years after Cyclone Aila. Sites of major embankment breaches are shown. Coloured circles reflect the location of sediment cores, measures of tidal sediment deposition, and GPS elevation points. Regional maps are shown in insets.

The low relative elevation of polders in southwest Bangladesh has been widely reported by studies of flood risk in the region[23], and is confirmed by Shuttle Radar Topography Mission (SRTM) elevation data and the direct measurements made here (Fig. 2 and Supplementary Fig. 1). Given these lowered landscapes, storm-surge flooding is one of the greatest threats facing the tidal delta plains of this region. On 25 May 2009, Cyclone Aila struck West Bengal, India, and southwest Bangladesh as a relatively weak Category 1 storm, causing embankment failures, tidal flooding and the displacement of >100,000 people in the areas of Koyra, Shyamnagar and Dacope[9,10] (Supplementary Fig. 1). At Polder 32 in Dacope, Aila caused five major breaches of the embankments that protect the island's western margin despite a storm-surge height just 0.5 m above the spring high-tide level (Supplementary Information and Fig. 7). Although the exact mechanism of failure at these locations remains uncertain, we note that: four of the five failures occurred at the mouths of former tidal channels blocked by the embankments; all breach sites had experienced ~50–200 m of riverbank erosion in the decade before the storm (Supplementary Fig. 8); and the breached tidal channels had scoured into fine sand at all sites (Fig. 3c,d). These attributes, and the fact that storm-surge height was well below the embankment tops (Fig. 2), suggest that the embankments failed either through collapse along over-steepened cut-banks or through undermining caused by hydraulic lift within shallow sands beneath the embankments at the former tidal channels. Within months after the storm, local repairs had closed several of the breaches (Supplementary Fig. 9), but inadequate construction led to nearly complete failure again in early 2010 (ref. 9). Although the history of embankment repair since the storm is complicated, 18–24 months passed before most of the breaches were soundly repaired.

During the roughly 2-year period before embankment repair, much of the polder was submerged on each high tide to a mean depth of 100 cm for an average of 9.8 h d^{-1} (Fig. 3 and Supplementary Fig. 5). In contrast, the adjacent Sundarbans, at ~100 cm higher, is inundated only during spring high tides (~37% of all tides) to a mean depth of just 20 cm for 1.7 h d^{-1}. The striking contrast between the tidal inundation patterns of these landscapes highlights the impact of sediment starvation and the historical loss of elevation, which has severely exacerbated the effects of tidal inundation by increasing the local tidal prism (volume of water moving on and off the polder). We calculate that the mean tidal cycle moved $\sim 62 \times 10^6$ m^3 of water through the breaches: four times more than if the elevation were the same as the adjacent Sundarbans.

Following the storm, the reactivated tidal channels scoured the breach sites, conveying sediment-laden water onto the polder, where broad splays of sand and mud were deposited (Fig. 3c). The alternating laminae of mud and sand indicate that deposition occurred primarily through tidal inundation, not by the initial storm surge (Fig. 3d and Supplementary Fig. 10). With the greater frequency and depth of inundation caused by the polder's low elevation, accelerated sedimentation rates led to an average of 37 cm of deposition in the two years following the storm, with many sites as high as 60–70 cm (Supplementary Information and Fig. 11). These values equate to a mean annual accretion rate of ~18 cm yr^{-1}, which is more than an order of magnitude higher than background sedimentation rates in the Sundarbans[8,18,25]. The high rates of sedimentation following embankment breaches exemplify the efficiency with which the Ganges–Brahmaputra fluvio-tidal system can disperse sediment to areas of accommodation, particularly where land has been starved of sediment for extended periods of time.

To understand the origin of elevation offset between the poldered landscape and Sundarbans, we establish a budget to account for differences among local, relative water levels and the natural and human-altered landscapes. The relative difference between local land-surface elevation and water levels (Δ_{RSL}) is defined by the rate of sediment aggradation (A) relative to eustatic sea-level rise (E), subsidence (M) and compaction (C), where $\Delta_{RSL} = A - (E + M + C)$ (ref. 1). We also account for the drying of shallow soils and anthropogenically enhanced rates of compaction resulting from wood extraction (W), as roots and stumps were removed for fuel and improved tilling following deforestation (Supplementary Table 1). In the case of the naturally flooded and forested Sundarbans, the mean Δ_{RSL} deterministically approaches ~0.0 ± 0.3 cm yr^{-1} (that is, no net change) because abundant sediment supply and regular tidal inundation compensate for local variation in compaction and subsidence. This net balance

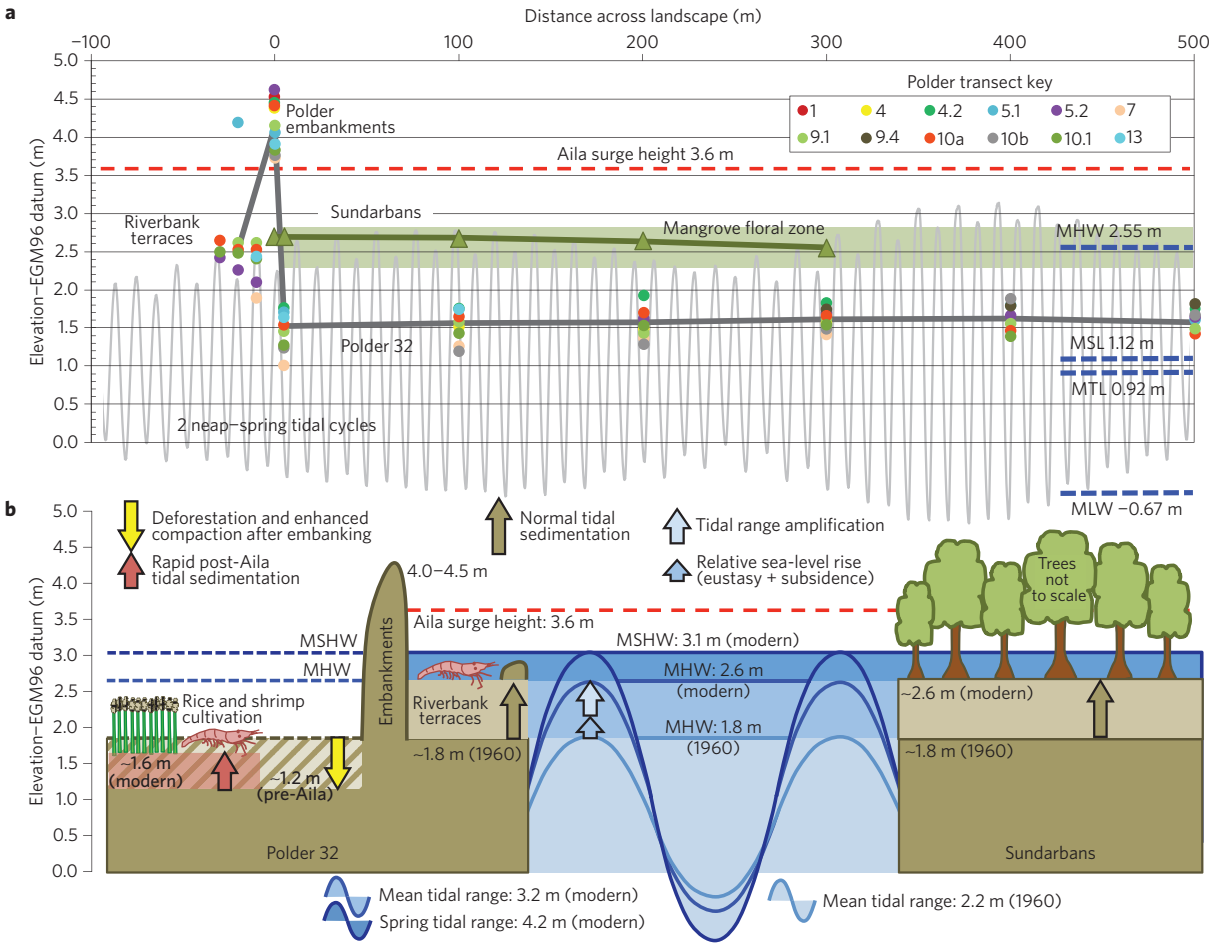

Figure 2 | Surface elevations and landscape model for Polder 32 and adjacent Sundarbans. a, GPS survey results for Polder 32, adjacent Sundarbans and tidal variations (see Supplementary Figs 2–4 for full data set and errors). **b**, Conceptual model for poldered and natural landscapes, with elevations for modern system and 1960 before poldering. Constructed embankments have mostly protected from severe flooding but led to sediment starvation, enhanced compaction, and tidal amplification[14], resulting in 1.0–1.5 m of elevation offset relative to mean high water and the nearby Sundarbans and riverbank terraces. MHSW, mean high spring water.

reflects the historical pattern of dynamic stability in this landscape where sediment accretion has remained in equilibrium with RSL rise[6,8,18] (Table 1).

In contrast, we calculate a Δ_{RSL} of -1.3 cm yr^{-1} for the sediment-starved polder, plus ~20 cm of lowering from wood extraction (W). These values account for 85 ± 35 cm of elevation loss in the 50 years since embankment construction (Table 1). However, the measured elevation difference is considerably higher at 105 ± 35 cm; if we further account for the 37 ± 18 cm of post-Aila sediment deposition, then the pre-storm elevation difference between the Sundarbans and the polder surface increases to 142 ± 53 cm. The resulting ~60 cm discrepancy between observed and calculated elevation offsets is too large to resolve by simply assuming higher rates of compaction, subsidence or wood extraction. Rather, we cite an additional loss term in the recently documented amplification of the tidal range (T) that has occurred in response to widespread embanking of the intertidal delta plain over the past 50 years[14]. This increase in tide levels accounts for a rise in MHW of 1.1 ± 0.4 cm yr^{-1}, or 55 ± 20 cm of elevation offset. Considered with the 85 ± 35 cm loss from compaction, subsidence and eustasy, this revised term for the effective rate of sea-level rise (Δ_{ERSL}) yields 140 ± 55 cm of relative water level increase, which matches closely the measured offset of 142 ± 53 cm between the Sundarbans and the pre-Aila polder surface. As noted in ref. 14, previous investigations considering only changes in mean sea level may not properly account for variations in MHW to which the mean landscape elevation is tied.

Although variation in the loss terms is important, we suggest that the most significant factor in lowered elevations of the polders has been the elimination of sediment delivery, because it removes the only mechanism for positive changes in land-surface elevation. To emphasize this point, we note that elevations of the Sundarbans and the riverbank terraces around the polder remain proximal to MHW (Figs 2 and 3), indicating that they have kept pace even with the enhanced rates of effective sea-level rise associated with tidal amplification[14]. With specific reference to the riverbank terraces, these narrow strips of land average >90 cm higher than the poldered surface inside the embankments, reflecting that they have been able to accrete at a rate comparable to local RSL owing to regular tidal inundation and sedimentation. Together, long-term stability of the Sundarbans and the equilibrium elevation of riverbank terraces reflect the robust capacity for the Ganges–Brahmaputra delta to disperse and aggrade sediment in response to historical and recently increased rates in the rise of effective sea level[14,24]. This capacity is further demonstrated by the ~18 cm yr^{-1} rate of sedimentation that occurred after tidal inundation was re-established on Polder 32 following Cyclone Aila.

Here we have detailed the impacts of Cyclone Aila on one of several affected polders[9,10], but the consequences of two years of daily tidal inundation are more related to the elevation deficit

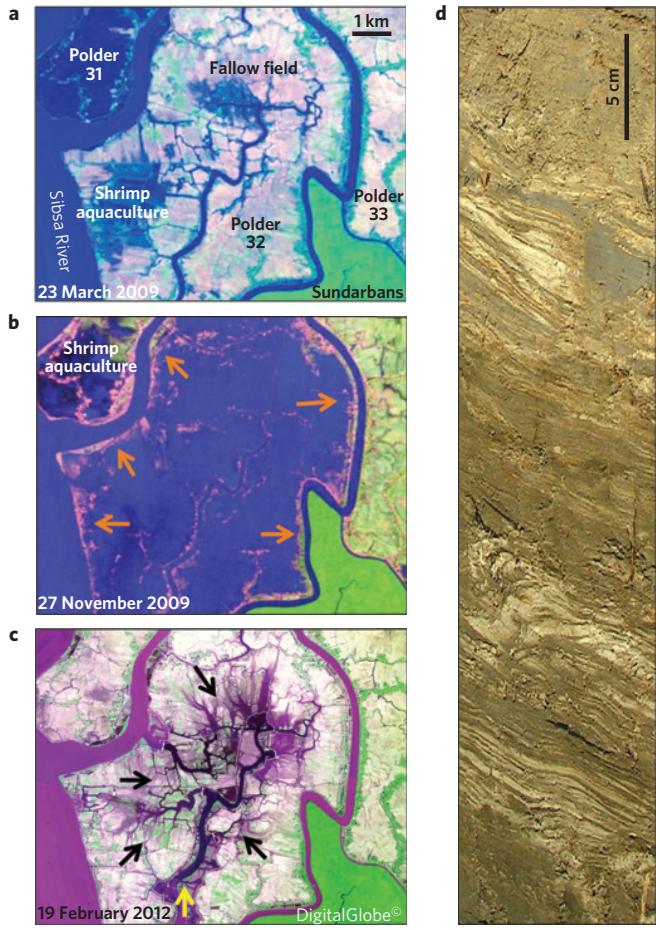

Figure 3 | Landsat and DigitalGlobe images of Polder 32 before and after embankment breaches and post-breach tidal-splay deposits. **a**, Dry-season image two months before Cyclone Aila showing the largely fallow landscape except for local shrimp aquaculture. **b**, High-tide, dry-season image six months after Aila showing inundation of Polder 32 by sediment-laden tidal waters, except for vegetated riverbank terraces (orange arrows). **c**, Dry-season, high-tide image 35 months after Aila when most embankments had been repaired, except for central tidal channel (yellow arrow). Remnant channel scours and tidal-splay deposits remain prominent (black arrows). **d**, Example of laminated fine sands and muds deposited during two years of regular tidal inundation.

caused by long-term sediment starvation than to this modest-strength storm. Although variability in the physical environment of southwest Bangladesh certainly exists, embanked islands of the region are more alike than different with many lying well below MHW (ref. 23; Supplementary Fig. 1). The processes and circumstances documented here implicate direct human modification of the environment as the most important agent of change in the western Ganges–Brahmaputra tidal delta plain, rather than global sea-level rise. However, the silver lining for Bangladesh and the delta system remains the one billion tons of river sediment that may be effectively dispersed onto the landscape to alleviate elevation deficits. On the basis of our observations, a feasible management strategy from the physical-science perspective may be to systematically breach embankment sections to facilitate sediment delivery and elevation recovery. Ultimately such an effort would require substantial coordination among government agencies, local stakeholders and international lenders, but there is potential to effectively steward these embanked landscapes through a variety of climate change scenarios.

Table 1 | Relative rates of vertical elevation change in the natural and embanked landscapes with net calculated and measured elevation changes for Polder 32.

Rates of vertical change*	Natural (Sundarbans)	Embanked (Polder 32)	Sources
Sediment accretion (A: cm yr^{-1})	1.1 ± 1.0	0.0 ± 0.1	Refs 7,8,18
Shallow compaction (C: cm yr^{-1})	0.4 ± 0.2	0.8 ± 0.3	Supplementary Fig. 12
Subsidence (M: cm yr^{-1})	0.3 ± 0.2	0.3 ± 0.2	Refs 14,25,27
Eustatic sea level (E: cm yr^{-1})	0.2 ± 0.1	0.2 ± 0.1	Refs 3,14
Subtotal (Δ_{RSL}: cm yr^{-1})	**0.0 ± 0.3**†	**−1.3 ± 0.7**	
Tidal amplification (T: cm yr^{-1})	1.1 ± 0.4	1.1 ± 0.4	Ref. 14
Total (Δ_{ERSL}: cm yr^{-1})	**0.0 ± 0.3**†	**−2.4 ± 1.1**	
Net elevation offset for Polder 32	**Calculated**	**Measured**	
Wood extraction (W: cm)	−20 ± 10	-	Supplementary Table 1
Δ_{RSL} over 50 years + W (cm)	−85 ± 45	-	
Δ_{ERSL} over 50 years + W (cm)	−140 ± 65	−142 ± 53‡	

*Derivation of values explained in Supplementary Information. †Net balance based on steady-state landscape and equilibrium. ‡Net elevation difference between Polder 32 and the adjacent Sundarbans in 2012 (105 ± 35 cm) less post-Aila sedimentation from 2009–2011 (37 ± 18 cm).

Methods

The fast-static GPS survey was conducted using two base stations comprising Trimble NetR9 receivers with Zephyr Geodetic 2 antennas. One antenna was mounted on a threaded rod cemented into the roof of a reinforced concrete school building. The other site comprised an antenna mounted on a heavy steel fixed-height tripod. Continuous GPS data for both base stations were processed using GAMIT version 10.4 to produce positions in the ITRF2008 reference frame. The positions were stabilized using GLOBK/GLORG with 21 IGS sites.

The rover was a Trimble NetR9 with a Zephyr Geodetic 2 antenna mounted on a fixed-height tripod. Observation times of at least 10 min were used for all rover data. While the rover was positioned on the embankment, a theodolite, also positioned on the embankment, was used to measure the relative elevations of the land inside and outside the embankment relative to the embankment and antenna. Theodolite errors were less than 1 cm. Elevation measurements were made at 150 sites along 18 transects extending 500–1500 m into the polder interior (Supplementary Fig. 2).

The GPS data were processed using Trimble Business Center, and the errors were estimated from adjusting the triangles formed by the rover and base stations. Elevation error for the base station was <2 cm and the median elevation error for all GPS points was 4 cm (Supplementary Figs 3,4). Only three points had errors of more than 10 cm. The ellipsoid height from GPS processing was converted to elevation relative to the EGM96 geoid model. We note that post-storm sedimentation has not been subtracted from the measured elevations owing to heterogeneities in deposit thickness and pre-existing topography, which would introduce an unknown degree of error.

A Schlumberger CTD Diver was deployed in the tidal channel adjacent to the eastern margin of Polder 32 (Fig. 1) from May 2012 to February 2013. Elevation of the CTD Diver was measured during the GPS levelling survey to tie water levels relative to land-surface elevations. Water level data (Supplementary Fig. 5) was used to calculate hydroperiods for both poldered and natural landscapes discussed in the text.

A 0.5 m gouge auger was used to collect sediment cores to 1.5 m depth at 114 locations on Polder 32, 11 sites on adjacent polders, and 2 sites in the Sundarbans (Fig. 1). Cores were collected along the GPS elevation survey transects to facilitate comparison of lithologic and topographic features of the landscape. Owing to the necessity for armed forest guards in the presence of tigers when

collecting Sundarban sediments, we were limited to two sediment cores on the natural Sundarban platform.

Dry-season penetrometer measurements were collected at five sites inside Polder 32, five sites on the riverbank terraces outboard of Polder 32, and two sites in the Sundarbans using an AMS 59000 dynamic cone penetrometer with a 45° vertex angle cone measuring 3.8 cm in diameter. Results of the penetrometer tests indicate that pre-Aila sediments within Polder 32 are more consolidated than sediments on the riverbank terraces and in the Sundarbans (Supplementary Fig. 12).

An estimate for elevation loss associated with wood extraction in poldered regions (that is, loss in root biomass on deforestation) was quantified using allometric equations developed in ref. 26 for estimating mangrove weight of trunk, leaf, above-ground and below-ground root biomass (Supplementary Information). Root weight of mangroves (W_R) is calculated as: $W_R = 0.199\rho^{0.899}D^{2.22}$ where ρ is species-specific wood density and D is trunk diameter at ~1.3 m height[26]. Measurements from approximately 40 mangrove trees (including *Heritiera fomes*, *Xylocarpus mekongensis*, *Avicennia* sp., *Bruguiera gymnorrhiza* and *Sonneratia apetala*; Supplementary Table 1) were obtained from the Sorbathkhali Forestry Station of the Sundarbans, where elevation and core transect data were measured (Fig. 1). Root volume (W_v) was calculated as: $(W_v) = W_R/1{,}000 * \rho$. The sum of root volume (302.2 m^3) divided by the area surveyed (~1,500 m^2) yields depth contributed by roots and below-ground biomass (~20 cm). Note that mangrove tree roots typically extend much deeper in the soil (1–2 m), and this calculated value should be considered total consolidated root depth (that is, minus inorganic sediment and pore space).

Changes in shoreline morphology on Polder 32 before and following Cyclone Aila were observed using Ikonos, Worldview and GeoEye images. Pre-cyclone shoreline morphologies were obtained from October 2001 Ikonos and April 2009 Worldview imagery. The post-cyclone shoreline morphology was obtained from GeoEye imagery collected in 2012. The high-water line visible on the landscape in each image was used to digitize the shorelines in ArcMap. Although it was not possible to correct the images for tidal stage, all observations were ground-truthed in the field, noting that the river margins where bank retreat was observed in the satellite images were characterized by steep-walled cut-banks consistent with measured bathymetry (Supplementary Fig. 8).

Received 11 March 2014; accepted 20 November 2014; published online 5 January 2015

References

1. Syvitski, J. P. M. *et al.* Sinking deltas due to human activities. *Nature Geosci.* **2,** 681–686 (2009).
2. IPCC *Climate Change 2013: The Physical Science Basis* (eds Stocker, T. F. *et al.*) (Cambridge Univ. Press, 2013).
3. Bhuiyan, M. J. A. N. & Dutta, D. Analysis of flood vulnerability and assessment of the impacts in coastal zones of Bangladesh due to potential sea-level rise. *Nature Hazards* **61,** 729–743 (2012).
4. Dasgupta, S., Huq, M., Sohel Masud, M., Mukherjee, N. & Pandey, K. Climate proofing infrastructure in Bangladesh: The incremental cost of limiting future flood damage. *J. Environ. Dev.* **20,** 167–190 (2011).
5. Brammer, H. Bangladesh's dynamic coastal regions and sea-level rise. *Clim. Risk Manage.* **1,** 51–62 (2014).
6. Allison, M. A. Historical changes in the Ganges–Brahmaputra delta front. *J. Coast. Res.* **14,** 1269–1275 (1998).
7. Goodbred, S. L. & Kuehl, S. A. Floodplain processes in the Bengal basin and the storage of Ganges–Brahmaputra river sediment: An accretion study using ^{137}Cs and ^{210}Pb geochronology. *Sedim. Geol.* **121,** 239–258 (1998).
8. Rogers, K. G., Goodbred, S. L. & Mondal, D. R. Monsoon sedimentation on the 'abandoned' tide-influenced Ganges–Brahmaputra Delta plain. *Estuar. Coast. Shelf Sci.* **131,** 297–309 (2013).
9. *Cyclone Aila: Joint UN Multi-Sector Assessment & Response Framework* 44 (United Nations, 2010).
10. Mehedi, H., Nag, A. K. & Farhana, S. *Climate Induced Displacement—Case Study of Cyclone Aila in the Southwest Coastal Region of Bangladesh* 37 (HumanityWatch, 2010).
11. Ericson, J., Vörösmarty, C., Dingman, S., Ward, L. B. & Meybeck, M. Effective sea-level rise and deltas: Causes of change and human dimension implications. *Glob. Planet. Change* **50,** 63–82 (2006).
12. Day, J. W., Pont, D., Hensel, P. F. & Ibañez, C. Impacts of sea-level rise on deltas in the Gulf of Mexico and the Mediterranean: The importance of pulsing events to sustainability. *Estuaries* **18,** 636–647 (1995).
13. Overeem, I. & Syvitski, J. P. M. *Dynamics and Vulnerability of Delta Systems* 54 LOICZ Reports Studies No. 35 (GKSS Research Center, LOICZ International Project Office, 2009).
14. Pethick, J. & Orford, J. D. Rapid rise in effective sea-level in southwest Bangladesh: Its causes and contemporary rates. *Glob. Planet. Change* **111,** 237–245 (2013).
15. Goodbred, S. L. & Kuehl, S. A. Holocene and modern sediment budgets for the Ganges–Brahmaputra river system: Evidence for highstand dispersal to flood-plain, shelf, and deep-sea depocenters. *Geology* **27,** 559–562 (1999).
16. Hanebuth, T. J. J., Kudrass, H. R., Linstadter, J., Islam, B. & Zander, A. M. Rapid coastal subsidence in the central Ganges–Brahmaputra Delta (Bangladesh) since the 17th century deduced from submerged salt-producing kilns. *Geology* 1–4 (2013).
17. Allison, M., Khan, S., Goodbred, S. & Kuehl, S. Stratigraphic evolution of the late Holocene Ganges–Brahmaputra lower delta plain. *Sedim. Geol.* **155,** 317–342 (2003).
18. Allison, M. & Kepple, E. Modern sediment supply to the lower delta plain of the Ganges–Brahmaputra River in Bangladesh. *Geo-Marine Lett.* **21,** 66–74 (2001).
19. Wilson, C. A. & Goodbred, S. L. Construction and maintenance of the Ganges–Brahmaputra–Meghna delta: Linking process, morphology, and stratigraphy. *Annu. Rev. Mar. Sci.* **7**, http://dx.doi.org/10.1146/annurev-marine-010213-135032 (2015).
20. Giri, C., Pengra, B., Zhu, Z., Singh, A. & Tieszen, L. L. Monitoring mangrove forest dynamics of the Sundarbans in Bangladesh and India using multi-temporal satellite data from 1973 to 2000. *Estuar. Coast. Shelf Sci.* **73,** 91–100 (2007).
21. Stanley, D. J. & Warne, A. G. Nile Delta in its destruction phase. *J. Coast. Res.* **14,** 794–825 (2012).
22. Day, J. W. *et al.* Restoration of the Mississippi Delta: Lessons from Hurricanes Katrina and Rita. *Science* **315,** 1679–1684 (2007).
23. Rahman, R. & Salehin, M. in *Disaster Risk Reduction. Approaches Bangladesh* (eds Shaw, R., Mallick, F. & Islam, A.) 65–90 (Springer, 2013).
24. Ellison, A. M., Mukherjee, B. B. & Karim, A. Testing patterns of zonation in mangroves: Scale dependence and environmental correlates in the Sundarbans of Bangladesh. *J. Ecol.* **88,** 813–824 (2000).
25. Goodbred, S. L. & Kuehl, S. A. The significance of large sediment supply, active tectonism, and eustasy on margin sequence development: Late Quaternary stratigraphy and evolution of the Ganges–Brahmaputra delta. *Sedim. Geol.* **133,** 227–248 (2000).
26. Komiyama, A., Poungparn, S. & Kato, S. Common allometric equations for estimating the tree weight of mangroves. *J. Trop. Ecol.* **21,** 471–477 (2005).
27. Stanley, D. J. & Hait, A. K. Holocene depositional patterns, neotectonics, and Sundarban mangroves in the western Ganges–Brahmaputra delta. *J. Coast. Res.* **16,** 26–39 (2000).

Acknowledgements

We thank D. Datta, B. Kumar, S. Hossain, Md R. Karim and F. Akter for their assistance with field data collection. As noted Figs 1, 3c, and Supplementary Fig. 8 include copyrighted material of DigitalGlobe, Inc., All Rights Reserved. Figure 3a,b includes Landsat imagery distributed by the Land Processes Distributed Active Archive Center (LP DAAC), located at USGS/EROS, Sioux Falls, South Dakota (http://lpdaac.usgs.gov). This research was financially supported by grants from the Office of Naval Research (N00014-11-1-0683) and National Science Foundation–Belmont Forum (No. 1342946). This paper is a contribution to the ICSU 2015 Sustainable Deltas Initiative.

Author contributions

All authors contributed extensively to the work presented in this paper. L.W.A., S.L.G.Jr, M.S.S. and D.R.M. designed the field project. L.W.A., S.L.G.Jr, D.R.M., C.A.W., K.R.A. and K.R. collected data. L.W.A., S.L.G.Jr, D.R.M., C.A.W., M.S.S. and C.S. processed and analysed data. L.W.A., S.L.G.Jr, C.A.W. and J.M.G. wrote the manuscript. L.W.A., S.L.G.Jr, D.R.M., M.S.S. and C.A.W. wrote the Supplementary Information. All authors discussed the results and implications and commented on the manuscript at all stages.

Additional information

Supplementary information is available in the online version of the paper. Reprints and permissions information is available online at www.nature.com/reprints. Correspondence and requests for materials should be addressed to S.L.G.Jr

Competing financial interests

The authors declare no competing financial interests.